

1 **Characterization, enrichment, and computational modeling of cross-linked actin**
2 **networks in trabecular meshwork cells**

3 Haiyan Li,¹ Devon H. Harvey,^{3,4} Jiannong Dai,^{3,4} Steven P. Swingle,² Anthony M Compton,¹
4 Chenna Kesavulu Sugali,^{3,4} Kamesh Dhamodaran,^{3,4} Jing Yao,⁵ Tsai-Yu Lin,⁵ Todd Sulchek,^{1,2}
5 Taeyoon Kim,⁶ C. Ross Ethier,^{1,2} Weiming Mao^{3,4,7,8,9}

6 **Affiliations**

- 7 1. Wallace H. Coulter Department of Biomedical Engineering, Georgia Institute of
8 Technology/Emory University, Atlanta, GA
9 2. Department of Mechanical Engineering, Georgia Institute of Technology, Atlanta, GA
10 3. Eugene and Marilyn Glick Eye Institute, Indiana University, Indianapolis, Indiana
11 4. Department of Ophthalmology, Indiana University, Indianapolis, Indiana
12 5. Department of Medical and Molecular Genetics, Indiana University, Indianapolis, Indiana
13 6. Weldon School of Biomedical Engineering, Purdue University, West Lafayette, Indiana.
14 7. Department of Biochemistry & Molecular Biology, Indiana University, Indianapolis,
15 Indiana
16 8. Department of Pharmacology and Toxicology, Indiana University, Indianapolis, Indiana
17 9. Stark Neurosciences Research Institute, Indiana University, Indianapolis, Indiana

18

19

20 **Abstract**

21 **Purpose**

22 Cross-linked actin networks (CLANs) are prevalent in the glaucomatous trabecular meshwork
23 (TM), yet their role in ocular hypertension remains unclear. We used a human TM cell line that
24 spontaneously forms fluorescently-labeled CLANs (GTM3L) to explore the origin of CLANs,
25 developed techniques to increase CLAN incidence in GMT3L cells, and computationally studied
26 the biomechanical properties of CLAN-containing cells.

27 **Methods**

28 GTM3L cells were fluorescently sorted for viral copy number analysis. CLAN incidence was
29 increased by (i) differential sorting of cells by adhesion, (ii) cell deswelling, and (iii) cell selection
30 based on cell stiffness. GTM3L cells were also cultured on glass or soft hydrogel to determine
31 substrate stiffness effects on CLAN incidence. Computational models were constructed to mimic
32 and study the biomechanical properties of CLANs.

33 **Results**

34 All GTM3L cells had an average of 1 viral copy per cell. LifeAct-GFP expression level did not
35 affect CLAN incidence rate, but CLAN rate was increased from ~0.28% to ~50% by a
36 combination of adhesion selection, cell deswelling, and cell stiffness-based sorting. Further,
37 GTM3L cells formed more CLANs on a stiff vs. a soft substrate. Computational modeling
38 predicted that CLANs contribute to higher cell stiffness, including increased resistance of the
39 nucleus to tensile stress when CLANs are physically linked to the nucleus.

40 **Conclusions**

41 It is possible to greatly enhance CLAN incidence in GTM3L cells. CLANs are mechanosensitive
42 structures that affect cell biomechanical properties. Further research is needed to determine the
43 effect of CLANs on TM biomechanics and mechanobiology as well as the etiology of CLAN
44 formation in the TM.

45 **Introduction**

46 Glaucoma, a major cause of blindness, is a common optic neuropathy in which retinal ganglion
47 cell dysfunction and damage result in characteristic patterns of visual field loss. Ocular
48 hypertension (OHT) is a major risk factor for glaucoma; moreover, it is the only treatable risk
49 factor. Ocular hypertension in primary open-angle glaucoma (POAG), the most common form of
50 glaucoma, is due to elevated aqueous humor outflow resistance, which in turn is most frequently
51 caused by pathological changes in the trabecular meshwork (TM) and inner wall of Schlemm's
52 canal (SC), as reviewed in (Stamer and Clark 2017).¹ Pathological findings in the TM associated
53 with OHT include: loss of TM cells,²⁻⁴ compromised TM cell function, excessive extracellular
54 matrix (ECM) deposition, and increased TM⁵⁻⁷ and ECM stiffness^{6, 8}. Despite these observations,
55 the fundamental causes of OHT remain unknown.

56 In addition to the pathological changes described above, it is known that cross-linked actin
57 networks (CLANs) are associated with OHT: they occur more frequently in TM cells from
58 glaucomatous eyes and can be induced by agents known to cause OHT, such as TGF- β 2 and
59 dexamethasone (DEX).⁹⁻¹⁶ These studies strongly suggest a functional link between CLANs and
60 OHT. CLANs consist of interconnected filamentous (F)-actin ("hub and spoke" morphology),
61 appearing as web-like (in 2D images) or spherical (in 3D images) intracellular structures.^{11, 12}
62 We and others have shown that CLANs colocalize with multiple proteins, including PIP2,
63 syndecan, α -actinin, filamin, PDLIM1, caldesmon, calponin, and tropomyosin.^{13, 17}

64 Despite the significant associations between CLANs and OHT/glaucoma, much remains
65 unknown about CLANs, including their impact on cellular functions, ECM production/remodeling,
66 mechanotransduction, and most importantly, intraocular pressure (IOP). These knowledge gaps
67 are due in part to experimental barriers. For example, it is difficult to induce and visualize
68 CLANs, and thus the reproducibility of CLAN studies has been challenging. Prior to our recent
69 paper, most previous CLAN-related research used primary human TM (pHTM) cells together

70 with glucocorticoid, TGF- β 2, or integrin activation, with the exception of some studies using
71 bovine TM cells.^{11-14, 16-20} These approaches have drawbacks; for example, CLAN induction rate
72 varies significantly between cell strains and even between batches from the same cell strain,
73 hindering reproducibility and rigor. Moreover, the use of primary cells is inherently limited by
74 passage numbers,²¹ making it challenging to conduct experiments that require significant
75 numbers of cells.

76 We recently described a unique TM cell line, GTM3-LifeAct-GFP (GTM3L). The GTM3L cell line
77 was derived from the widely-used GTM3 cell line, established about 20 years ago by
78 immortalizing glaucomatous pHTM cells.^{22, 23} GTM3 cells share many features with pHTM cells,
79 including phagocytic capability and DEX-inducible myocilin expression.²⁴⁻²⁶ We serendipitously
80 discovered the GTM3L subline, which spontaneously forms fluorescently labelled CLANs
81 suitable for live imaging.²² Using these cells, we showed that CLANs make TM cells stiffer, less
82 dynamic, and more resistant to latrunculin-B (an actin polymerization inhibitor).²²

83 Interestingly, not all GTM3L cells form CLANs.²² To further study CLANs using GTM3L cells, it
84 is important to be able to enrich CLAN+ cells beyond their spontaneous low incidence rate
85 (defined as the number of CLAN+ cells divided by the total number of cells) reported in GTM3L
86 cells²². In this study, we explored the potential origin of CLANs, combined several methods to
87 increase CLAN incidence rate in GMT3L cells with validation of their effects on cell stiffness,
88 and developed a computational model to study the biomechanical impact of CLANs on cells.

89

90 **Methods**

91 **Cell culture**

92 GTM3L cells were cultured in low-glucose Dulbecco's Modified Eagle's Medium (DMEM; Gibco,
93 Thermo Fisher Scientific, Waltham, MA, USA) or Opti-MEM (Thermo Fisher Scientific)

94 containing 10% fetal bovine serum (FBS; HyClone, Thermo Fisher Scientific) and 1%
95 penicillin/streptomycin/glutamine (PSG; Gibco/Thermo Fisher Scientific), and maintained at
96 37°C in a humidified atmosphere with 5% CO₂. Fresh media was supplied every 2-3 days.

97 **Fluorescence-activated sorting and Lentiviral copy number analysis**

98 About 2 x 10⁷ GTM3L cells were sorted into 3 groups with high, medium, and low GFP intensity
99 using a BD FACSAria™ III Cell Sorter (BD, Franklin Lakes, NJ) at the core facility at Indiana
100 University (Supplemental Figure 1). These cells were cultured, and DNA was isolated using a
101 Nucelospin kit (Macherey-Nael) for viral copy number analysis. The copy number of the lentiviral
102 vector sequence in the Woodchuck Hepatitis Virus Posttranscriptional Regulatory Element
103 (WPRE) was normalized to the copy number of the host cell's ApoB genomic sequence using
104 droplet digital PCR (Bio-rad, Hercules, CA). The primers, PCR conditions, and reagents are
105 listed in Supplemental Materials.

106 **Hydrogel preparation**

107 The hydrogel precursor gelatin methacryloyl (GelMA [6% w/v final concentration], Advanced
108 BioMatrix, Carlsbad, CA, USA) was mixed with lithium phenyl-2,4,6-
109 trimethylbenzoylphosphinate (LAP, 0.075% w/v final concentration) photoinitiator (Sigma-Aldrich,
110 Saint Louis, MO). Thirty microliters of the hydrogel solution were pipetted onto Surfasil-coated
111 (Thermo Fisher Scientific) 18 × 18-mm square glass coverslips followed by placing 12-mm
112 round silanized glass coverslips on top to facilitate even spreading of the polymer solution.
113 Hydrogels were crosslinked by exposure to UV light (CL-3000 UV Crosslinker; Analytik Jena,
114 Germany) at 1J/cm². The hydrogel-adhered coverslips were removed with fine-tipped tweezers
115 and placed hydrogel-side facing up in 24-well culture plates (Corning; Thermo Fisher Scientific).

116 **Osmotic deswelling of GTM3L cells**

117 GTM3L cells were seeded at 3×10^4 cells/cm² atop either glass coverslips or soft hydrogels and
118 cultured in DMEM with 10% FBS and 1% PSG overnight. Then, GTM3L cells were cultured in
119 DMEM with 1% FBS and 1% PSG and exposed to 2% Polyethylene glycol 300 (PEG300; Sigma)
120 for 2 or 5 days.

121 **Live cell imaging**

122 Live imaging was used to determine how long CLANs persisted after PEG300 removal. CLANs
123 were defined as “F-actin–containing cytoskeletal structures with at least one triangulated actin
124 arrangement consisting of actin spokes and at least three identifiable hubs.”¹⁸

125 GTM3L cells were seeded in either a 35 mm dish with a 0.17 mm thick glass bottom (World
126 Precision Instruments, Sarasota, FL) or on a glass chip (chip ID: CGF400800F; ARRALYZE -
127 part of LPKF Group, Garbsen, Germany) which was mounted on a 35mm plastic dish with a 22
128 mm square cutout in the center. The glass chip contained 512 microwells of 400 μ m diameter
129 and 162 microwells of 800 μ m diameter. The bottom of the microwell was about 175 μ m thick,
130 and the height of the wall of the microwell was about 475 μ m. The behavior of cells on both
131 substrates was similar and the data we present combines experiments from both substrates.
132 The cells were cultured in serum-free OptiMEM supplemented with 1%
133 glutamine/penicillin/streptomycin. On treatment day 0, the cells were treated with 2% PEG300
134 (Catalog # 202371, Sigma Aldrich). The cells then were monitored daily for the formation of
135 CLANs, which most often formed between treatment days 4-6. Once CLANs were identified,
136 treatment was withdrawn by gently replacing the medium containing 3% PEG300 with fresh
137 culture media without PEG300. Cells were immediately transferred to and were maintained in a
138 stage top incubator (Tokai, Shizuoka-ken, Japan) secured on the stage of a Nikon Eclipse Ti2
139 inverted microscope (Nikon, Melville, NY) set at 5% CO₂ and 37°C for the duration of live
140 imaging. Time lapse images were immediately captured using a 40x objective S plan fluor

141 ELWD objective (Nikon). Further images were captured every 30 seconds for the first 2 hours
142 and then at every minute for an additional 4 hours.

143 **Image analysis**

144 To determine the persistence time of CLANs after PEG300 withdrawal, five researchers
145 individually analyzed the captured images. The time at which CLANs were no longer visible was
146 recorded, and the average time over the 5 observers was taken as the persistence time of
147 CLANs after PEG300 withdrawal. For this part of the study, our definition of visible CLANs was
148 identical to that described above in “Live cell imaging”.

149 **Cell sorting based on cell-substrate adherence**

150 GTM3L cells were plated in T75 flasks and grown to confluence in DMEM with 10% FBS and 1%
151 PSG. 2 ml of 0.25% trypsin was added and incubated for 2 min at 37°C, and non-adherent cells
152 and media were discarded. The remaining adherent cells were then released by adding a
153 further 2 ml of 0.25% trypsin for 30 s, adding media to neutralize the trypsin, centrifugation for
154 10 min at 1000g, and resuspending the pellet in DMEM with 10% FBS and 1% PSG. The cells
155 were then seeded on glass coverslips for testing osmotic deswelling-induced CLAN formation.

156 **Cell sorting based on cell stiffness**

157 GTM3L cells were selected by stiffness according to an established protocol.²⁷⁻³¹ In brief, 2 ml of
158 a GTM3L cell suspension (1.8×10^6 cells/ml) were passed through a microfluidic device with a
159 narrow channel designed with 14, 7 μm constrictions angled at 30° that direct the trajectory of
160 cells, and thus fractionate cells, depending on their stiffness. This device was made from PDMS
161 (Sylgard 184; Thermo Fisher Scientific) cured on an SU-8 photoresist mold etched using
162 standard photolithography procedures. The day before sorting, devices were passivated with 1%
163 Pluronic F-68 solution (Thermo Fisher Scientific). Cells suspended in flow buffer (culture media
164 with 20% Percoll to provide neutral buoyancy to cells and 0.4 mg/ml DNase I to avoid DNA-

165 induced blockage if cells lyse) were flowed into the device at 3-7 $\mu\text{l}/\text{min}$ and were collected from
166 the device outlets (each corresponding to a different stiffness), while control samples were
167 taken from unperfused cells. Samples were spun down and resuspended in 150 μl of fresh
168 culture media, and the suspended cells were plated and expanded.

169 **Atomic force microscopy**

170 An MFD-3D AFM (Asylum Research, Santa Barbara, CA, USA) was used to make cell stiffness
171 measurements using silicon nitride cantilevers with an attached borosilicate sphere (diameter =
172 10 μm ; nominal spring constant = 0.1 N/m; Novascan Technologies, Inc., Ames, IA, USA).
173 Cantilevers were calibrated by measuring the thermally induced motion of the unloaded
174 cantilever before measurements. The indentation depth was limited to 400 nm to avoid
175 substrate effects and the tip velocity was adjusted to 800 nm/s to avoid viscous effects.³² Five
176 measurements/cell were conducted, and at least 5 cells were measured/group. For hydrogel
177 stiffness measurement, a force map covering a 40 x 40 μm area (5 x 5 grid of points) was
178 measured. Data from AFM measurements were fitted to the Hertz model to calculate the
179 effective Young's Modulus of the cells, assuming a Poisson's ratio of 0.5.

180 **Immunostaining**

181 GTM3L cells were fixed with 4% paraformaldehyde (Electron Microscopy Sciences, Hatfield, PA,
182 USA) at room temperature for 20 min, permeabilized with 0.5% Triton™ X-100 (Thermo Fisher
183 Scientific) and incubated with Phalloidin-iFluor or 594 (Cell Signaling Technology, Danvers, MA,
184 USA)/DAPI according to the manufacturer's instructions. Coverslips were mounted with
185 ProLong™ Gold Antifade (Invitrogen) on Superfrost™ microscope slides (Theromo Fisher
186 Scientific), and fluorescent images were acquired with a Leica DM6 B upright microscope
187 system. Images were captured from at least 10 fields per group, which corresponds to over a

188 thousand cells. The images were subsequently analyzed to determine the percentage of CLAN+
189 cells, calculated as the ratio of the number of CLAN+ cells to the total number of cells.

190 **Computational modeling**

191 To simulate CLAN-like networks, we employed our agent-based model with F-actin and actin
192 cross-linking protein (ACP) simplified via cylindrical segments.³³⁻³⁶ (Supplemental Figure 2) A
193 cell nucleus was included in some simulations, represented as a triangulated mesh. The
194 positions of all points defining the cylindrical segments and the triangulated mesh were updated
195 in each time step using the Langevin equation and the forward Euler integration scheme. For all
196 elements, extensional, bending, and repulsive forces were considered as deterministic forces.
197 For the nucleus, forces enforcing conservation of volume and surface area were also
198 considered. F-actins were assembled via nucleation with specific orientations and
199 polymerization, but they did not undergo depolymerization. Actin cross-linking proteins
200 interconnected pairs of F-actins to form functional cross-linking points.

201 Via the self-assembly process of F-actin and ACP, CLAN-like networks were created. In
202 simulations without the cell nucleus, the CLAN-like network was formed in a thin rectangular
203 domain ($10 \times 8.66 \times 0.1 \mu\text{m}$) with periodic boundary conditions in the x and y directions. The
204 actin concentration (C_A) was $100 \mu\text{M}$, and the molar ratios of ACPs ($R_{ACP} = C_{ACP}/C_A$) was 0.1.
205 After network assembly, the periodic boundary condition was disabled in the y direction. Then,
206 F-actins crossing the two boundaries normal to the y direction were severed, and their ends
207 were clamped to the boundaries. For bulk rheology measurement, the +y boundary was
208 displaced in either the +x, +y, or -y directions at a constant rate to apply shear, tensile, or
209 compressive strain to the network, respectively, while the -y boundary was fixed. The maximum
210 strain was 0.05, and the strain rate was 0.001 s^{-1} . At each strain level, stress was calculated by
211 summing the component of forces acting on the ends of all F-actins clamped on the +y
212 boundary and then dividing the sum by the boundary area. For shear stress, the x component of

213 forces was used, but for tensile and compressive stresses, the y component was used.
214 Simulations with the cell nucleus were performed in a larger rectangular domain with or without
215 the CLAN-like network. The CLAN-like network was created along the nucleus surface as
216 explained earlier, in a three-dimensional rectangular domain ($10 \times 10 \times 5.1 \mu\text{m}$). Note that the
217 initial z dimension of the domain is close to the diameter of the nucleus, $5 \mu\text{m}$. The actin
218 structure was created right above the nucleus (i.e., within a space defined by a radial distance
219 from the nucleus center between r_N and $1.1 \times r_N$ where r_N is a nucleus radius). During the actin
220 assembly, the nucleus was frozen without a change in its spherical shape. C_A was $60 \mu\text{M}$, which
221 was calculated using the space for actin assembly. R_{ACP} was 0.1. After network assembly,
222 compressive strain was applied to the +y boundary, whereas the -y boundary was fixed. The
223 maximum compressive strain was -0.2 (i.e., 20% decrease in the z dimension of the domain),
224 and the strain rate is -0.01 s^{-1} . In each strain level, a total resistant force exerted by the actin
225 structure and the nucleus was measured, and then stress was calculated by dividing the total
226 force by the contact area between the nucleus and the boundary. Further details of the agent-
227 based model and parameters used in simulations are given in Supplemental Materials.

228

229 **Statistical analysis**

230 GraphPad Prism software v10.2.3 (GraphPad Software, La Jolla, CA, USA) was used for all
231 analyses. All data sets were tested for normality using the Shapiro-Wilk test and were confirmed
232 to meet the normality criteria. The significance level was set at $p < 0.05$. Comparisons between
233 groups were assessed by t-tests and one-way analysis of variance (ANOVA) with Tukey's
234 multiple comparisons post hoc tests.

235

236 **Results**

237 **GTM3L cells had 1 viral insertion per cell on average**

238 Although the original GTM3 cells were monoclonal, after lentiviral (pLenti-LifeAct-EGFP-BlastR)
239 ³⁷ transduction and antibiotic selection, GTM3L cells were established to be polyclonal and
240 observed to have variable GFP intensities. We hypothesized this variation was related to
241 different expression levels of the LifeAct-GFP fusion protein and conducted studies to test this
242 hypothesis.

243 We sorted GTM3L cells into 3 groups with high, medium, and low GFP intensity, respectively
244 (Supplemental Figure 1). These cells were cultured, and DNA was isolated for viral copy
245 number analysis. We found that naïve GTM3 cells had negligible viral copy number per cell,
246 with readings at background levels. In contrast, all 3 groups of GTM3L cells had 1 viral copy per
247 cell on average (**Table 1**), regardless of their GFP intensity, suggesting that the number of viral
248 copy/insertions per cell was not correlated with LifeAct-GFP expression levels.

249 We found that CLAN formation rate was very low among all 3 groups of GTM3L cells described
250 previously (high, medium, and low GFP intensities), and was similar to unsorted GTM3L cells
251 (data not shown). Since CLANs were relatively easy to identify in GTM3L cells with medium and
252 high GFP expression, these two groups of cells were used in subsequent studies.

253

254 **Enrichment of CLAN-forming cells based on cell-substrate adhesion, osmotic deswelling**
255 **and cell stiffness**

256 *Enrichment of CLAN+ cells based on cell-substrate adhesion*

257 It has been observed that interactions between cells and substrates can enhance the formation
258 of CLANs in TM cells.^{17, 19, 38} This insight led us to employ an adhesion-based selection strategy
259 to augment the proportion of CLAN+ cells. We noted that after 9 cycles of selecting GTM3L

260 cells with stronger substrate attachment, there was a remarkable increase in the frequency of
261 CLAN+ cells, rising from a low incidence of $0.28 \pm 0.42\%$ to $4.16 \pm 2.95\%$ (**Figure 1A**). The
262 CLAN incidence rate in unselected cells was somewhat higher, albeit still small, vs. that seen in
263 the original GTM3L cells (0.04%)²², which is likely due to the use of GTM3-high GFP expression
264 cells (described above)

265 *Enrichment of CLAN+ cells using PEG300*

266 Studies have shown that macromolecular crowding induced by PEG promotes CLAN formation
267 in an acellular actin filament solution modeling system.^{39, 40} We hypothesized that cell shrinkage
268 induced by PEG would also facilitate CLAN formation in GTM3L cells. To investigate the effect
269 of cellular crowding on CLAN formation in GTM3L cells, cells that had undergone 9 cycles of
270 adhesion-based selection (see above) were treated with 2% PEG300 for either 2 or 5 days,
271 after which we quantified the incidence rate of CLAN+ cells. As expected, GTM3L cells exposed
272 to PEG300 shrank (**Figure 1A and B**). Additionally, there was a marked increase in the
273 incidence of CLAN+ cells compared to the control group, i.e. vs. cells that had been enriched by
274 selecting for adhesion but without PEG300 deswelling (**Figure 1B**). Specifically, the CLAN+
275 incidence rate was $4.16 \pm 2.95\%$ in control cells, which increased to $11.80 \pm 3.58\%$ and $26.50 \pm$
276 7.51% after 2- and 5-days of PEG300 treatment, respectively (**Figure 1B and C**).

277 We further studied whether withdrawal of PEG300 would lead to loss of CLANs. GTM3L cells
278 were treated with PEG300 for 4-7 days to induce CLAN formation, followed by replacement of
279 the PEG300-containing culture media with PEG-free media. We observed a time-dependent
280 loss of CLANs after PEG300 withdrawal (**Figure 2A-H and supplemental video**). Interestingly,
281 while CLAN formation required several days, most of the PEG300-induced CLANs were lost
282 within a few hours after PEG300 withdrawal (CLAN persistence = 58.94 ± 61.70 min [mean \pm
283 SD], N=31 cells; **Figure 2I**).

284

285 **Enrichment of CLAN+ cells based on cell stiffness**

286 We recently showed that GTM3L cells containing CLANs are stiffer than cells without CLANs.²²
287 Therefore, we asked whether we could further enrich CLAN+ cells using a well-established
288 microfluidic device that sorts cells depending on their stiffness.²⁷⁻³¹ GTM3L cells, after
289 undergoing 9 cycles of adhesion-based selection, were passed through this device, which
290 contains a narrow channel with angled constrictions that direct cells along a stiffness-dependent
291 trajectory, thereby sorting cells into four groups according to their stiffness. We note that no
292 cells were obtained from one of the five outlets, and thus have only 4 groups which we denote
293 as extra soft, soft, medium, and stiff. Note that these categorizations do not map onto cellular
294 Young's modulus values definable *a priori*, since the sorting process depends on cell stiffness,
295 channel geometry, and cell size and shape.²⁷⁻³¹ To evaluate the capability of these sorted cells
296 to form CLANs, we then subjected them to a 5-day treatment with PEG300, using unsorted cells
297 as a control. We established an association between the stiffness of GTM3L cells, based on the
298 microfluidic-based cell sorting, and their ability to form CLANs. Specifically, we observed a
299 significant elevation in CLAN formation as cell stiffness increased (**Figure 3A**).

300 Together, using a combination of all 3 CLAN+ cell enrichment methods (9 cycles of adhesion-
301 based selection, cell sorting based on cell stiffness, and PEG300 treatment), we created a
302 GTM3L sub-population containing about 50% CLAN+ cells (**Figure 3A**). This represents a
303 significant enrichment from the original 0.28% CLAN+ incidence in GTM3L cells.

304

305 **Confirmation of cell stiffening in enriched GTM3L cells**

306 Motivated by our previous findings that CLAN+ GTM3L cells are stiffer than CLAN- GTM3L cells
307 and naïve GTM3 cells²², we also measured cell stiffness using AFM. We noted that in both our

308 current and previous ²² studies, the CLAN+ GTM3L cells were reported to have a stiffness of
309 approximately 4 kPa. Importantly, we confirmed that CLAN+ cells were stiffer than CLAN- cells
310 (N=4 cells/group, $p < 0.05$) (**Figure 3B**). This strengthens our confidence in our approach to
311 selecting CLAN+ cells from a mixed population.

312

313 **Substrate stiffness influences CLAN incidence in GTM3L cells**

314 Substrate stiffness has been shown to affect cell stiffness, with cells adapting by increasing their
315 own stiffness in response to being cultured on a more rigid substrate.^{41, 42} In our study, we
316 observed a notable correlation between the stiffness of cells and the presence of CLANs.
317 Therefore, we hypothesized that substrate stiffness might also impact the formation of CLANs in
318 GTM3L cells. To explore this hypothesis, we cultured stiff GTM3L cells, enriched through
319 adhesion-based and cell stiffness selection steps (see above), on two different substrates: soft
320 hydrogels with a stiffness of approximately 2.36 kPa, and stiff glass coverslips. The cells were
321 then treated with PEG300 for 5 days. We observed that GTM3L cells cultured on the stiff
322 substrate exhibited a significantly elevated incidence of CLAN+ cells ($p < 0.0001$) (**Figure 4**).

323

324 **The mechanical properties of CLAN-like networks and CLAN-containing nucleus**

325 To further study the impact of CLANs on cell biomechanics, we used agent-based models to
326 probe the rheological properties of CLANs and the role of CLANs in cell stiffening. First, we
327 created a CLAN-like network with a triangular lattice geometry (**Figure 5A**) and performed bulk
328 rheology measurements imposing shear, tensile, and compressive strains on the network
329 (**Figure 5B**). We found that network stiffness was greatest when delivering tensile strain and the
330 smallest when delivering shear strain (**Figure 5B**), implying that CLANs in cells resist tensile
331 deformation effectively. Next, we performed simulations with only a cell nucleus or with a cell

332 nucleus surrounded by CLANs with or without physical links between the nucleus and CLANs
333 (**Figure 5C and D**). When compressive strain was applied to the two types of structures,
334 resistance to compression was higher when there were physical links between the nucleus and
335 CLANs (**Figure 5C and D**). This implies that it is more difficult to deform the nucleus in the
336 presence of CLANs, which is consistent with the increase in cell stiffness measured
337 experimentally by AFM.

338

339 **Discussion**

340 In this study, we sought to understand various features of the enigmatic actin structures known
341 as CLANs, which occur in TM cells and are associated with ocular hypertension. Towards this
342 end, we used our previously reported GTM3L cells, which spontaneously form GFP-labelled
343 CLANs in some cells. Fortunately, we were able to combine several methods to increase the
344 incidence rate of CLAN+ GTM3L cells, successfully obtaining a subpopulation of GTM3L cells
345 with ~50% CLAN incidence rate. This significant enrichment of CLAN+ cells will be a valuable
346 tool in future work, since it provides a large population of CLAN-positive cells to work with.

347 We also asked whether the amount of transgene expression in GTM3L cells was associated
348 with the extent of lentiviral integration into the host cell's genome. To our surprise, we found that
349 all GTM3L cells, regardless of their transgene expression levels, had on average only one
350 lentiviral insertion/integration event per cell. Generally, lentiviral integration sites in host
351 chromosomes are random, and high dose of lentiviruses (more than 1 copy per cell) can insert
352 at multiple regions in the host cell genome.^{43, 44}

353 The above finding led us to the hypothesis that the presence or absence of CLANs in GTM3L
354 cells depends on the locus of lentiviral insertion rather than the number of insertions. The
355 rationale for this hypothesis includes the following:

- 356 • It is well known that lentiviruses integrate at random sites as well as at certain “hot spots” in
357 the genome. Since the original GTM3 cells are monoclonal and all GTM3L cells were
358 cultured in the same extracellular environment, the most likely explanation for CLAN
359 formation is the difference in lentiviral integration sites.
- 360 • Different from the monoclonal GTM3 cells, our GTM3L cells are polyclonal, i.e. we did not
361 conduct clonal selection or expansion after transduction. We observed a very low and
362 unpredictable CLAN formation rate in GTM3L cells: sometimes there were many CLAN+
363 cells in a well, and sometimes there were no CLAN+ cells at all. This observation is
364 consistent with our hypothesis and suggests that only a few lentiviral integration patterns will
365 trigger CLAN formation.

366 Overall, the formation of CLANs in GTM3L cells may require two “hits”. We hypothesized that
367 GTM3L cells with certain lentiviral insertion/integration pattern(s) are prone to form CLANs.
368 When these cells grow in an unfavorable environment for CLAN formation, they form only a few
369 CLANs (~0.28%), yet if they grow in a favorable environment, such as on a stiff substrate or in
370 the presence of PEG300, they form significantly more CLANs.

371 We were able to enrich the population of CLAN+ cells using different methods: differential
372 substrate adhesion, PEG300 exposure and cell stiffness-based sorting. Interestingly, these
373 methods were synergistic, suggesting that they might be selecting for different CLAN-associated
374 phenotypes. The timescale associated with PEG300 exposure was noteworthy, since the
375 induction of CLANs by PEG300 took several days, yet CLAN disassembly after PEG300
376 removal occurred within hours. We do not understand the cause of this difference, nor do we
377 understand the exact mechanism by which PEG300 induces CLANs in TM cells. The simplest
378 possibility is that cell deswelling by PEG300 leads to cytoplasmic molecular crowding, an effect
379 that was seen in an acellular model where crowding decreased α -actinin binding to F-actin and
380 possibly led to F-actin thinning and shortening.⁴⁰ Another possibility is that PEG300 exposure
381 leads to cellular stress, and that CLAN formation is a generic stress response of TM cells. For

382 example, the formation of CLANs at the perinuclear region might provide TM cells with
383 additional mechanical shielding or stabilization. This idea that CLANs as a stress response may
384 also help explain the observation that CLANs tend to form more on stiffer substrates, as well as
385 in the presence of DEX and TGF- β 2. More experiments are clearly needed to explore this
386 concept.

387 We employed an agent-based computational model to understand why CLAN+ cells are stiffer.
388 We hypothesized that CLAN+ cells exhibit higher stiffness because their nuclei are harder to
389 deform due to the surrounding CLANs. To test this hypothesis, we first computationally
390 measured the rheological properties of CLAN-like networks and found that the networks resisted
391 tensile deformation effectively. Then, we applied compressive deformation to a simplified cell
392 nucleus with or without CLANs and found that the presence of CLANs resulted in much higher
393 resistance of the cell nucleus to compression due to high tensile resistance of CLANs;
394 specifically, deformation of the cell nucleus was hindered by the limited extensibility of actin
395 fibers. Based on these observations, which are consistent with our hypothesis, it is likely that the
396 higher stiffness of CLAN+ cells partially originates from CLANs around the nucleus.

397 Probably the most important question about CLANs is whether they directly contribute to
398 decreased outflow facility and hence elevated IOP, or are simply an associated epiphenomenon.
399 Our data do not directly answer this question; even the finding that a stiff substrate, such as
400 seen in the TM of ocular hypertensive eyes, promotes CLAN formation is consistent with both
401 possibilities. To address this question will require more work in a variety of models, and we
402 suggest that our findings can play an important role by motivating and facilitating cell-based
403 models. For example, one possibility would be to decellularize TM tissue in perfused anterior
404 segments and then repopulate the TM by magnetically steering CLAN+ cells into the TM.
405 Another approach would be to use an artificial outflow pathway construct (TM-on-a-chip),
406 populating the construct with CLAN+ cells to determine effects on flow resistance. All such

407 studies will require large numbers of CLAN+ cells, the production of which will be greatly
408 facilitated by our enrichment strategies. Also, if the gene(s) that promotes CLAN formation are
409 discovered (e.g. by comparing CLAN- vs. CLAN+ GTM3L cells using DNAseq), CLAN formation
410 can be induced in the mouse TM and the effect of CLANs on outflow facility and IOP can be
411 determined in vivo.

412 Of course, this work is subject to certain limitations. Besides the lack of outflow facility and IOP
413 data, key among these is that the GTM3L cells are derived from a transformed cell line (GTM
414 cells). It is well known that the biology of transformed TM cells is different from primary TM
415 cells.²¹ However, we believe these GTM3L are still a valuable tool for studying CLANs because
416 of several reasons.

- 417 1. Important features are consistent between GTM3L CLAN+ cells and pHTM CLAN+ cells,
418 such as resistance to actin relaxing reagents^{16, 22} and increased cell stiffness.²²
- 419 2. Our GTM3L cells form CLANs spontaneously, offering several advantages:
 - 420 • Live imaging of CLAN+ cells under physiological conditions.
 - 421 • Enriched CLAN+ GTM3L cell populations make omics-based studies possible.
 - 422 • Our GTM3L cell line has unlimited proliferation capability, and CLAN formation in this line is
423 spatially consistent (predominantly in the perinuclear region), which improves
424 reproducibility.
- 425 3. LifeAct-GFP expression does not affect TM cell biomechanical properties. Unlike human
426 mesenchymal stem cells,⁴⁵ our GTM3L cells did not demonstrate adverse effects since
427 CLAN- GTM3L cells and GTM3 cells showed similar stiffness and viscosity.
- 428 4. Our cell culture studies are directly intellectually linked to functional outcomes in whole eyes.
429 Specifically, we know that increased TM tissue stiffness is associated with OHT^{5, 6} and
430 impaired IOP homeostasis, which in view of the greater stiffness of GTM3L CLAN+ cells,
431 strongly suggests mechanistic link(s) between CLANs and OHT. In future, we fully expect to

432 be able to translate our findings from GTM3L cells into whole eyes.

433 In summary, we have developed an effective strategy to greatly increase the presence of
434 CLAN+ cells in our newly discovered GTM3L subline. Based on our findings, we believe that
435 CLANs, either induced by glaucomatous signals (elevated TGF β 2, elevated cortisone or steroid
436 treatment, or elevated IOP/mechanical stretching) or even as a primary initiating factor of
437 glaucoma, lead to pathological changes in TM cell biology, biomechanics, and mechanobiology,
438 resulting in OHT in glaucomatous eyes. Further research is needed to determine these changes
439 and the underlying mechanisms, and this subline will be a useful tool for this purpose.

440

441 **Acknowledgements**

442 Supported by the National Institute of Health/National Eye Institute Award Numbers
443 R01EY026962 (WM), R01EY031700 (WM), R21EY033929 (WM) and R01EY031710 (CRE);
444 BrightFocus Foundation G2023009S (WM); a challenge grant from Research to Prevent
445 Blindness (Department of Ophthalmology, Indiana University School of Medicine); the Georgia
446 Research Alliance (CRE); as well as National Science Foundation Award Number 2134701 (TS)
447 and CBET-2225476 (TS).

448 The authors thank Dr. Kenneth Cornetta of the Gene Therapy Testing Laboratory at Indiana
449 University School of Medicine for ddPCR resources.

450 The content is solely the responsibility of the authors and does not necessarily represent the
451 official views of the National Institutes of Health.

452 **REFERENCES**

- 453 1. Stamer WD, Clark AF. The many faces of the trabecular meshwork cell. *Exp Eye Res*
454 2017;158:112-123.
- 455 2. Alvarado J, Murphy C, Juster R. Trabecular meshwork cellularity in primary open-angle
456 glaucoma and nonglaucomatous normals. *Ophthalmology* 1984;91:564-579.
- 457 3. Grierson I, Howes RC. Age-related depletion of the cell population in the human
458 trabecular meshwork. *Eye (Lond)* 1987;1 (Pt 2):204-210.
- 459 4. Kuehn MH, Vranka JA, Wadkins D, Jackson T, Cheng L, Ledolter J. Circumferential
460 trabecular meshwork cell density in the human eye. *Exp Eye Res* 2021;205:108494.
- 461 5. Last JA, Pan T, Ding Y, et al. Elastic modulus determination of normal and
462 glaucomatous human trabecular meshwork. *Invest Ophthalmol Vis Sci* 2011;52:2147-2152.
- 463 6. Raghunathan VK, Benoit J, Kasetti R, et al. Glaucomatous cell derived matrices
464 differentially modulate non-glaucomatous trabecular meshwork cellular behavior. *Acta Biomater*
465 2018;71:444-459.
- 466 7. Vahabikashi A, Gelman A, Dong B, et al. Increased stiffness and flow resistance of the
467 inner wall of Schlemm's canal in glaucomatous human eyes. *Proc Natl Acad Sci U S A*
468 2019;116:26555-26563.
- 469 8. Raghunathan VK, Morgan JT, Park SA, et al. Dexamethasone Stiffens Trabecular
470 Meshwork, Trabecular Meshwork Cells, and Matrix. *Invest Ophthalmol Vis Sci* 2015;56:4447-
471 4459.
- 472 9. Tripathi RC, Li J, Chan WF, Tripathi BJ. Aqueous humor in glaucomatous eyes contains
473 an increased level of TGF-beta 2. *Exp Eye Res* 1994;59:723-727.
- 474 10. Armaly MF, Becker B. Intraocular pressure response to topical corticosteroids. *Fed Proc*
475 1965;24:1274-1278.
- 476 11. Clark AF, Miggans ST, Wilson K, Browder S, McCartney MD. Cytoskeletal changes in
477 cultured human glaucoma trabecular meshwork cells. *J Glaucoma* 1995;4:183-188.
- 478 12. Clark AF, Wilson K, McCartney MD, Miggans ST, Kunkle M, Howe W. Glucocorticoid-
479 induced formation of cross-linked actin networks in cultured human trabecular meshwork cells.
480 *Invest Ophthalmol Vis Sci* 1994;35:281-294.
- 481 13. Bermudez JY WH PG, Yan LJ, Clark AF, Mao W. Two-dimensional differential in-gel
482 electrophoresis (2D-DIGE) reveals proteins associated with cross-linked actin networks in
483 human trabecular meshwork cells. *J Clin Exp Ophthalmol* 2016.
- 484 14. Hoare MJ, Grierson I, Brotchie D, Pollock N, Cracknell K, Clark AF. Cross-linked actin
485 networks (CLANs) in the trabecular meshwork of the normal and glaucomatous human eye in
486 situ. *Invest Ophthalmol Vis Sci* 2009;50:1255-1263.
- 487 15. O'Reilly S, Pollock N, Currie L, Paraoan L, Clark AF, Grierson I. Inducers of cross-linked
488 actin networks in trabecular meshwork cells. *Invest Ophthalmol Vis Sci* 2011;52:7316-7324.
- 489 16. Montecchi-Palmer M, Bermudez JY, Webber HC, Patel GC, Clark AF, Mao W. TGFbeta2
490 Induces the Formation of Cross-Linked Actin Networks (CLANs) in Human
491 Trabecular Meshwork Cells Through the Smad and Non-Smad Dependent Pathways. *Invest*
492 *Ophthalmol Vis Sci* 2017;58:1288-1295.
- 493 17. Filla MS, Woods A, Kaufman PL, Peters DM. Beta1 and beta3 integrins cooperate to
494 induce syndecan-4-containing cross-linked actin networks in human trabecular meshwork cells.
495 *Invest Ophthalmol Vis Sci* 2006;47:1956-1967.
- 496 18. Wade NC, Grierson I, O'Reilly S, et al. Cross-linked actin networks (CLANs) in bovine
497 trabecular meshwork cells. *Exp Eye Res* 2009;89:648-659.
- 498 19. Filla MS, Schwinn MK, Nosie AK, Clark RW, Peters DM. Dexamethasone-associated
499 cross-linked actin network formation in human trabecular meshwork cells involves beta3 integrin
500 signaling. *Invest Ophthalmol Vis Sci* 2011;52:2952-2959.

- 501 20. Filla MS, Clark R, Peters DM. A syndecan-4 binding peptide derived from laminin 5 uses
502 a novel PKCepsilon pathway to induce cross-linked actin network (CLAN) formation in human
503 trabecular meshwork (HTM) cells. *Exp Cell Res* 2014;327:171-182.
- 504 21. Keller KE, Bhattacharya SK, Borrás T, et al. Consensus recommendations for trabecular
505 meshwork cell isolation, characterization and culture. *Exp Eye Res* 2018;171:164-173.
- 506 22. Peng M, Rayana NP, Dai J, et al. Cross-linked actin networks (CLANs) affect stiffness
507 and/or actin dynamics in transgenic transformed and primary human trabecular meshwork cells.
508 *Exp Eye Res* 2022;220:109097.
- 509 23. Pang IH, Shade DL, Clark AF, Steely HT, DeSantis L. Preliminary characterization of a
510 transformed cell strain derived from human trabecular meshwork. *Curr Eye Res* 1994;13:51-63.
- 511 24. Jain A, Wordinger RJ, Yorio T, Clark AF. Spliceosome protein (SRp) regulation of
512 glucocorticoid receptor isoforms and glucocorticoid response in human trabecular meshwork
513 cells. *Invest Ophthalmol Vis Sci* 2012;53:857-866.
- 514 25. Chen W, Yang X, Fang J, Zhang Y, Zhu W, Yang X. Rho-Associated Protein Kinase
515 Inhibitor Treatment Promotes Proliferation and Phagocytosis in Trabecular Meshwork Cells.
516 *Front Pharmacol* 2020;11:302.
- 517 26. Gasull X, Castany M, Castellanos A, et al. The LRRC8-mediated volume-regulated
518 anion channel is altered in glaucoma. *Sci Rep* 2019;9:5392.
- 519 27. Islam M, Brink H, Blanche S, et al. Microfluidic Sorting of Cells by Viability Based on
520 Differences in Cell Stiffness. *Sci Rep* 2017;7:1997.
- 521 28. Wang G, Mao W, Byler R, et al. Stiffness dependent separation of cells in a microfluidic
522 device. *PLoS One* 2013;8:e75901.
- 523 29. Stone NE, Raj A, Young KM, et al. Label-free microfluidic enrichment of cancer cells
524 from non-cancer cells in ascites. *Sci Rep* 2021;11:18032.
- 525 30. Islam M, Mezencev R, McFarland B, et al. Microfluidic cell sorting by stiffness to
526 examine heterogenic responses of cancer cells to chemotherapy. *Cell Death Dis* 2018;9:239.
- 527 31. Wang G, Turbyfield C, Crawford K, Alexeev A, Sulchek T. Cellular enrichment through
528 microfluidic fractionation based on cell biomechanical properties. *Microfluid Nanofluidics*
529 2015;19:987-993.
- 530 32. Vargas-Pinto R, Gong H, Vahabikashi A, Johnson M. The effect of the endothelial cell
531 cortex on atomic force microscopy measurements. *Biophys J* 2013;105:300-309.
- 532 33. Li J, Biel T, Lomada P, Yu Q, Kim T. Buckling-induced F-actin fragmentation modulates
533 the contraction of active cytoskeletal networks. *Soft matter* 2017;13:3213-3220.
- 534 34. Jung W, P Murrell M, Kim T. F-actin cross-linking enhances the stability of force
535 generation in disordered actomyosin networks. *Comput Part Mech* 2015;2:317-327.
- 536 35. Kim T, Hwang W, Lee H, Kamm RD. Computational analysis of viscoelastic properties of
537 crosslinked actin networks. *PLoS computational biology* 2009;5:e1000439.
- 538 36. Mak M, Zaman MH, Kamm RD, Kim T. Interplay of active processes modulates tension
539 and drives phase transition in self-renewing, motor-driven cytoskeletal networks. *Nat Commun*
540 2016;7:10323.
- 541 37. Padilla-Rodriguez M, Parker SS, Adams DG, et al. The actin cytoskeletal architecture of
542 estrogen receptor positive breast cancer cells suppresses invasion. *Nat Commun* 2018;9:2980.
- 543 38. Filla MS, Schwinn MK, Sheibani N, Kaufman PL, Peters DM. Regulation of cross-linked
544 actin network (CLAN) formation in human trabecular meshwork (HTM) cells by convergence of
545 distinct beta1 and beta3 integrin pathways. *Invest Ophthalmol Vis Sci* 2009;50:5723-5731.
- 546 39. Huber F, Strehle D, Schnauß J, Käs J. Formation of regularly spaced networks as a
547 general feature of actin bundle condensation by entropic forces. *New Journal of Physics*
548 2015;17:043029.
- 549 40. Park J, Lee M, Lee B, Castaneda N, Tetard L, Kang EH. Crowding tunes the
550 organization and mechanics of actin bundles formed by crosslinking proteins. *FEBS Lett*
551 2021;595:26-40.

- 552 41. Janmey PA, Fletcher DA, Reinhart-King CA. Stiffness Sensing by Cells. *Physiological*
553 *Reviews* 2020;100:695-724.
- 554 42. Solon J, Levental I, Sengupta K, Georges PC, Janmey PA. Fibroblast adaptation and
555 stiffness matching to soft elastic substrates. *Biophys J* 2007;93:4453-4461.
- 556 43. Mitchell RS, Beitzel BF, Schroder AR, et al. Retroviral DNA integration: ASLV, HIV, and
557 MLV show distinct target site preferences. *PLoS Biol* 2004;2:E234.
- 558 44. Schroder AR, Shinn P, Chen H, Berry C, Ecker JR, Bushman F. HIV-1 integration in the
559 human genome favors active genes and local hotspots. *Cell* 2002;110:521-529.
- 560 45. Flores LR, Keeling MC, Zhang X, Sliogeryte K, Gavara N. Lifeact-GFP alters F-actin
561 organization, cellular morphology and biophysical behaviour. *Sci Rep* 2019;9:3241.

562

563

564 **Figure legend**

565

566 **Figure 1. Enrichment of CLAN+ GTM3L cells using adhesion-based selection and PEG300**

567 **deswelling. (A)** Representative fluorescence micrographs of F-actin in GTM3L cells before and
568 after 9 cycles of adhesion-based selection, with nuclei and F-actin labelling shown in blue and
569 grey, respectively. The green inset in A shows a zoomed-in view of F-actin that does not form a
570 CLAN. The red inset in B shows a zoomed-in view of F-actin in a CLAN. Scale bars, 10 μm . **(B)**
571 Representative fluorescence micrographs of F-actin in GTM3L cells that underwent 9 cycles of
572 adhesion-based selection and were then subjected to PEG300 treatment for either 2 or 5 days.
573 Nuclei and F-actin are labelled in blue and grey, respectively. Scale bar, 20 μm . **(C)** Analysis of
574 the percentage of CLAN+ cells caused by treatment with PEG300 for 2 and 5 days ($n = 40$
575 images from 12 experimental replicates for the control group, $n = 20$ images/group from 6
576 experimental replicates for the groups treated with 2% PEG300). The bars and error bars
577 indicate means \pm standard deviations. Significance was determined by one-way ANOVA using
578 multiple comparisons tests. ****: $p < 0.0001$.

579

580 **Figure 2. The persistence of CLANs after PEG300 withdrawal. (A-H)** Images of a GTM3L
581 cell at various times after PEG300 was removed from cells by medium change. Arrowheads
582 denote CLANs in live cells. Scale bar: 50 μm . **(I)** The persistence time of CLANs after PEG300
583 withdrawal, as assayed in in 31 GTM3L cells. Bars: mean and SD.

584

585 **Figure 3. Enrichment of CLAN+ GTM3L cells based on cell stiffness. (A)** GTM3L cells, after
586 9 cycles of adhesion-based selection, were sorted into four groups according to their stiffness:
587 extra soft, soft, medium, and stiff. Control cells were unsorted cells. Each group of cells were
588 plated on coverslips and exposed to 2% PEG300 for 5 days. The incidence rate of CLAN+ cells

589 was quantified in each cell group ($n = 10$ images/group from 3 experimental replicates). The
590 violin plot shows medians as horizontal solid lines and the interquartile range as dashed lines.
591 Significance was determined by one-way ANOVA using multiple comparisons tests. ****:
592 $p < 0.0001$. **(B)** Stiffness of CLAN+ and CLAN- cells in an enriched GTM3L cell population was
593 measured by AFM with a $10 \mu\text{m}$ tip ($n = 4$ cells/group). The bars and error bars indicate means
594 \pm standard deviations. Significance was determined by unpaired Student's t-test. *: $p < 0.05$.

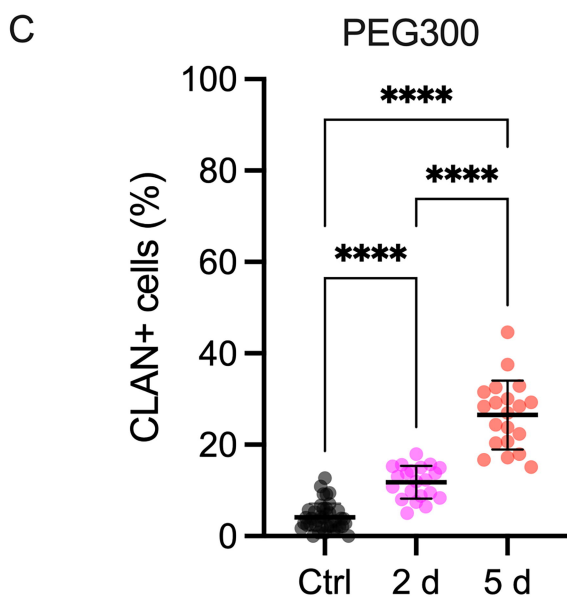
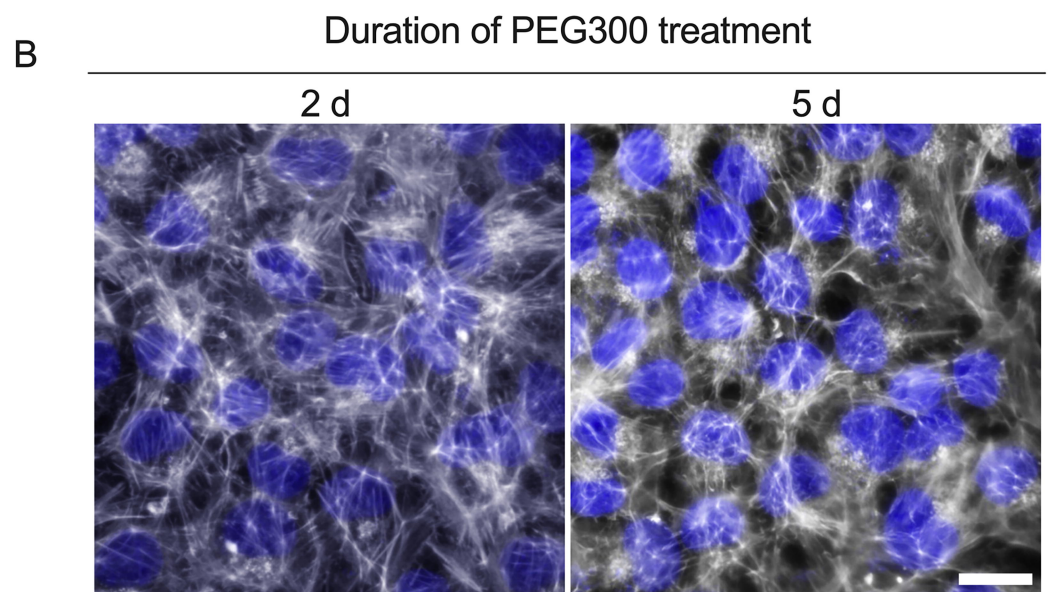
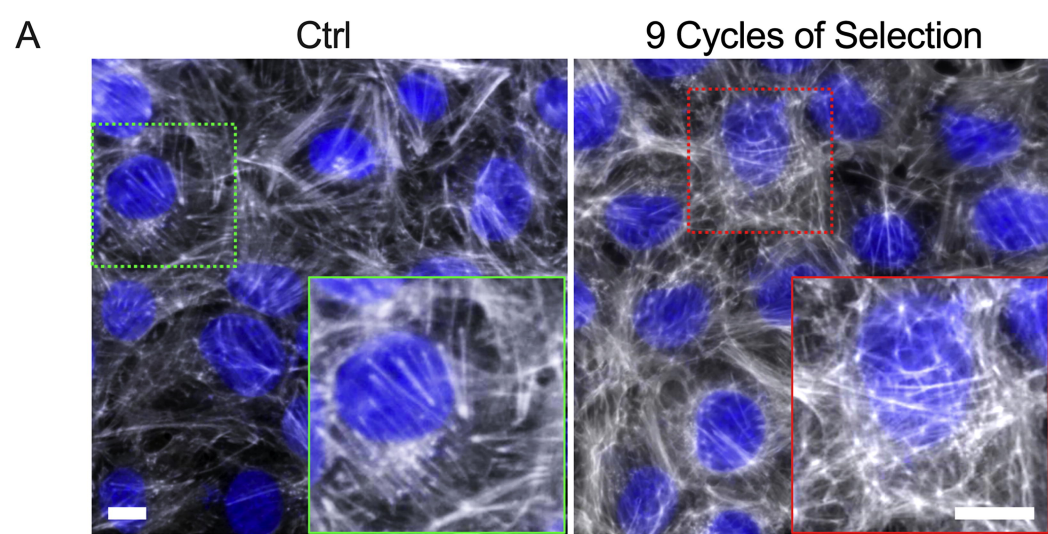
595

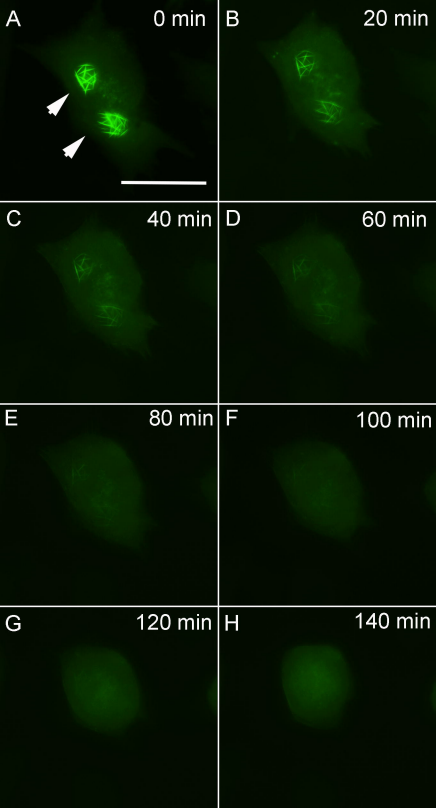
596 **Figure 4. Substrate stiffness affects CLAN formation. (A)** Representative fluorescence
597 micrographs showing F-actin in GTM3L cells, with CLAN incidence rate enriched through
598 adhesion- and cell stiffness-based selection. Cells were cultured on either glass coverslips or
599 soft hydrogels (2.36 kPa). Nuclei are labelled in blue. Scale bar, $20 \mu\text{m}$. **(B)** Incidence rate of
600 CLAN+ cells as a function of substrate stiffness ($n = 10$ images/group from 3 experimental
601 replicates). The bars and error bars indicate means \pm standard deviations. Significance was
602 determined by unpaired Student's t-test. ****: $p < 0.0001$.

603

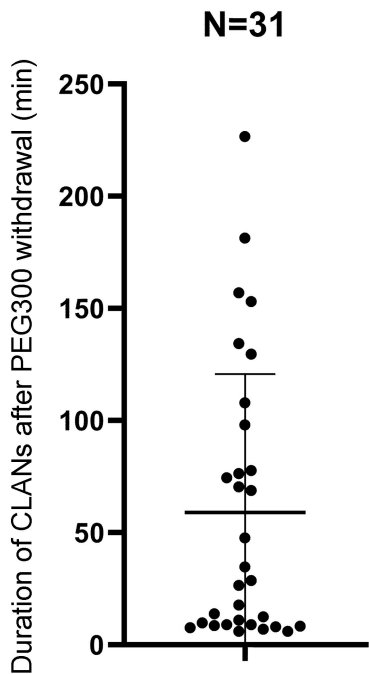
604 **Figure 5. Simulations of the biomechanical effects of CLAN-like networks. (A)** A CLAN-like
605 network consisting of F-actin (red) and actin cross-linking proteins (ACPs, yellow) created in a
606 thin rectangular domain. **(B)** Stiffness of the CLAN-like network in (A) in response to shear,
607 tensile, and compressive deformations. The bars and error bars indicate means \pm standard
608 deviations ($N=10$). Significance was determined by one-way ANOVA and Tukey post-hoc test
609 with $p < 0.0001$ by pairwise comparison between deformation types. **(C)** Snapshots of the
610 nucleus with or without CLANs before and after the application of compressive normal strain up
611 to $\epsilon = -0.5$. In the case with CLANs, there are physical links between a fraction (20%) of F-actins
612 and the nucleus. Colors in the actin fibers indicate the relative tensile force that fiber is bearing.

613 Compressive forces are considered zero force and shown in blue. **(D)** Stress calculated from
614 the resistant force developed during compressive deformations. The bars and error bars
615 indicate means \pm standard deviations (N=10). Significance was determined by one-way ANOVA
616 and Tukey post-hoc test with $p < 0.0001$ by pairwise comparison between conditions.

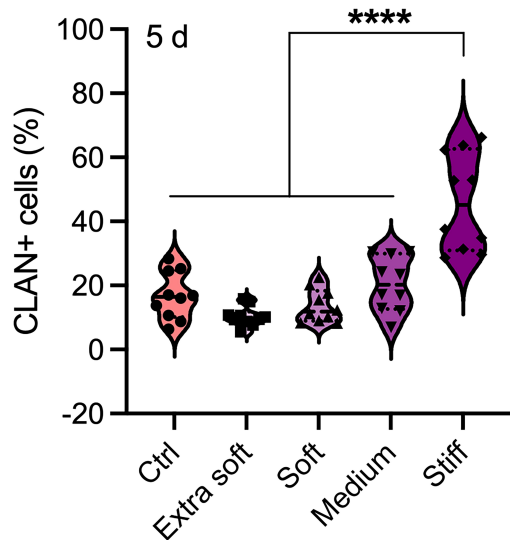




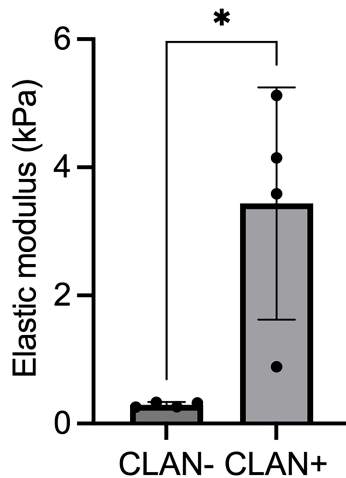
I



A Cell stiffness selection + PEG300

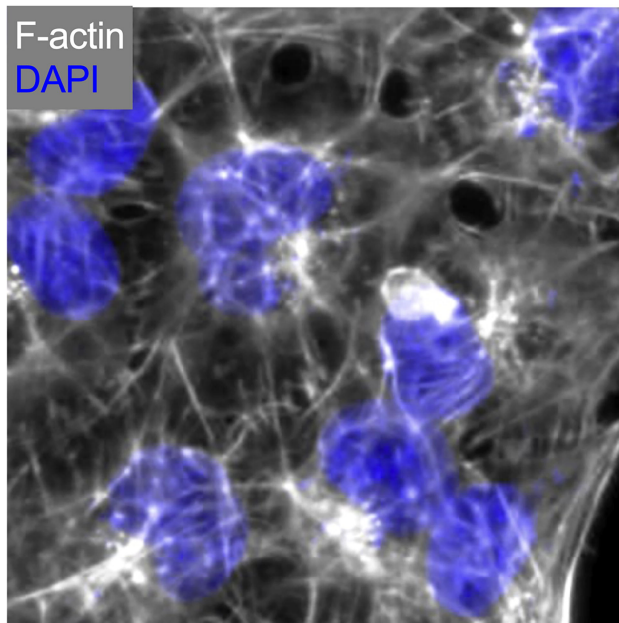


B Cell stiffness measurement by AFM

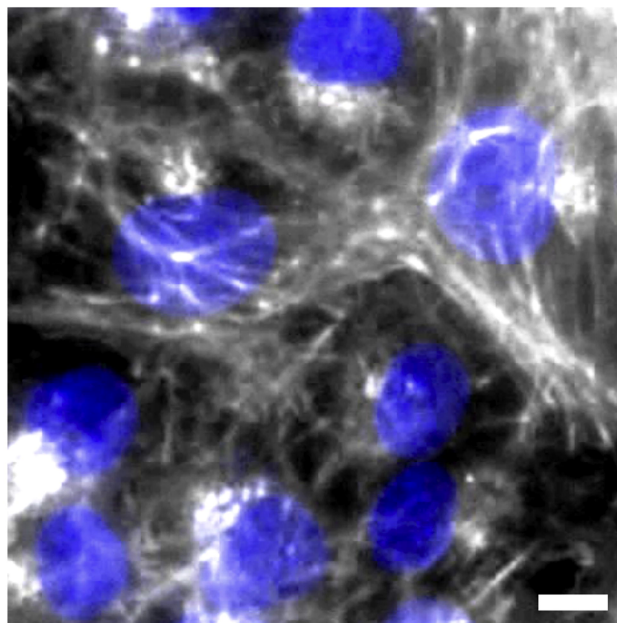


A

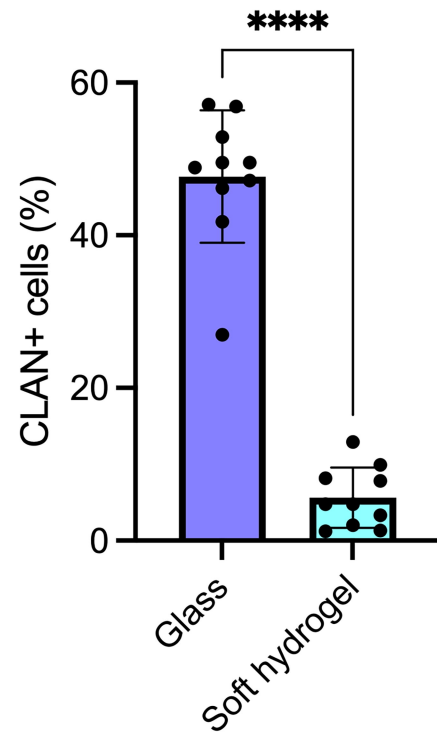
Glass

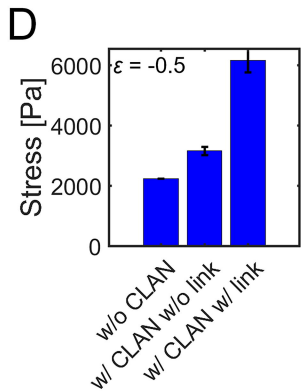
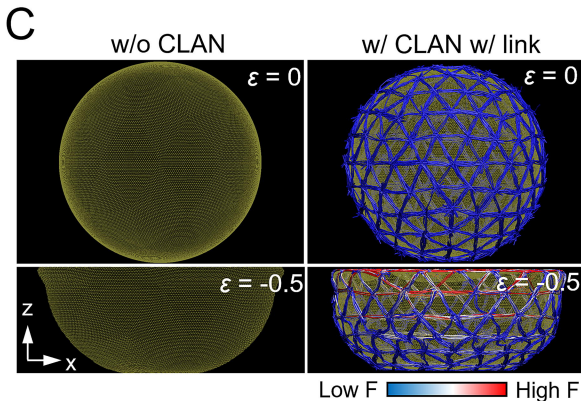
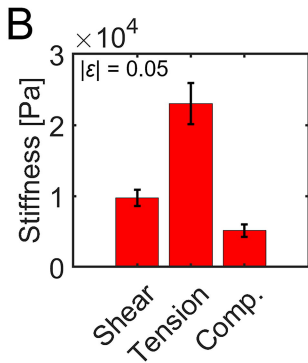
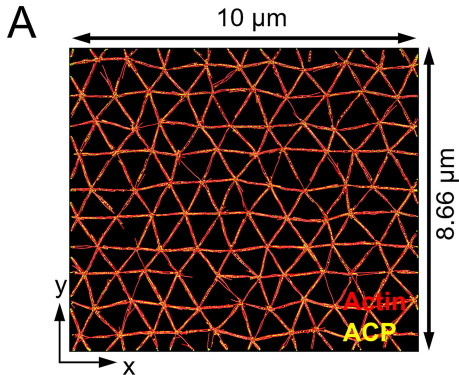


Soft hydrogel



B





Cells	Average viral copy number per cell
Naïve GTM3 (negative control)	9.0439×10^{-05}
GTM3L high GFP intensity	1.0999
GTM3L medium GFP intensity	1.1299
GTM3L low GFP intensity	1.1320

Table 1. Average viral copy number per GTM3L cell.